

Highly Stable Dye-Sensitized Solar Cell using Cobalt Tris(bipyridyl) Complexes via Monolithic Architecture

Jorge Martins^{a,b}, Ana M.V.M. Pereira^{a,b}, Seyedali Emami^{a,b}, Carlos Manuel Silva^c, Dzmitry Ivanou^{a,b*}, Adélio Mendes^{a,b*}

^aLEPABE - Laboratory for Process, Environment, Biotechnology and Energy, Department of Chemical Engineering, Faculty of Engineering of University of Porto, Rua Dr. Roberto Frias s/n 4200-465 Porto, Portugal

^bALICE - Associate Laboratory in Chemical Engineering, Faculty of Engineering of University of Porto, Rua Dr. Roberto Frias s/n 4200-465 Porto, Portugal

^cCICECO - Aveiro Institute of Materials, Department of Chemistry, University of Aveiro, Campus Universitário de Santiago, 3810-193 Aveiro, Portugal

*corresponding author: ivanou@fe.up.pt (Dzmitry Ivanou); mendes@fe.up.pt (Adélio Mendes)

Abstract:

This study reports on the exceptional stability of cobalt-mediated dye-sensitized solar cells (DSSCs) assembled in a monolithic configuration with a carbon counter electrode (CE). DSSCs using $[\text{Co}(\text{bpy})_3]^{2+/3+}$ redox mediators often face stability challenges due to light-induced interaction with *tert*-butylpyridine (TBP), an electrolyte additive. This leads to the loss of electrochemically active mediators and degradation of the photovoltaic performance. However, the monolithic DSSCs in this work demonstrated unprecedented stability under continuous light soaking for over 1000 hours. The stability is attributed to the device architecture and the carbon CE, which mitigate critical degradation mechanisms. Additionally, its adsorption capacity and opacity reduce the amount of free TBP in the electrolyte, thereby suppressing harmful photoinduced $[\text{Co}(\text{bpy})_3]^{3+}$ -TBP complexation and water-induced redox reactions. Despite high TBP concentrations (1.2 M), which typically accelerate degradation in conventional DSSCs, the monolithic devices maintained their performance due to electrolyte retention and reduced ion diffusion within the porous carbon layer. This study highlights the critical role of architecture in stabilizing cobalt-mediated DSSCs, paving the way for robust, long-term energy conversion applications.

Keywords: Dye-Sensitized Solar Cells; M-DSSC; Cobalt redox mediator; Electrolyte; Stability; Carbon Counter electrode

1. Introduction

Dye-sensitized solar cells (DSSCs) are a promising photovoltaic (PV) technology that has attracted research interest due to the use of inexpensive materials, straightforward manufacturing, and aesthetically appealing design. Recently, DSSCs have experienced a resurgence in scientific development and commercialization to address the need for off-grid power in low-power electronics operating in low-light conditions [1]. High power conversion efficiencies (PCEs) above 30 % have been achieved under artificial indoor light [2].

The use of transition-metal complexes such as cobalt (II/III) complexes allows for enhancing the power conversion efficiency (PCE) of DSSCs. These complexes present low light absorption in the visible range, are less corrosive, and present more positive redox potential, which reduces the overpotential for dye regeneration and enables higher open-circuit voltages (V_{oc}) [3-5]. Yella *et al.* obtained a PCE of 11.9 % using cobalt bipyridine complexes ($[Co(bpy)_3]^{2+/3+}$) and porphyrin dye YD2-o-C8, with a V_{oc} of 0.965 V [6]; the PCE of cobalt-mediated devices increased to 12.5 % by co-sensitization with organic dye Y123. Organic and porphyrin dyes have a donor- π -bridge-acceptor structure that can be easily tuned to optimize the light absorption efficiency and reduce the recombination losses, leading to higher PCEs [7]. Kakiage *et al.* employed a co-sensitization strategy using ADEKA-1 and LEG4 organic dye and a multi-capping treatment of the dye-sensitized TiO_2 layer using eight different molecules with various alkyl-chain lengths and with three kinds of anchor moieties (carboxy, phosphonic, and silyl groups). This approach, together with optimized cobalt trisphenanthroline complexes ($[Co(phen)_3]^{2+/3+}$) electrolyte, resulted in a high V_{oc} of 1.013 V and a high PCE of 14.3 % [8].

Despite the advantages of cobalt redox mediators, they display slow redox kinetics, which accelerates electron recombination from TiO_2 to the Co(III). Furthermore, their bulky molecular structure hinders charge diffusion, leading to the accumulation of Co(III) species at the photoanode/electrolyte interface [3,9]. This increases back electron recombination, reducing the photocurrent and V_{oc} [10].

Additives such as tert-butylpyridine (TBP) are introduced into the electrolyte to mitigate recombination; TBP passivates the TiO_2 surface, upshifting its conduction band and shielding the oxidized cobalt species from electron transfer [11-13].

TBP is essential for obtaining highly efficient devices with cobalt-mediated electrolytes. However, although TBP enhances PCE, it also undermines the stability of DSSCs by coordinating with and reacting with $[\text{Co}(\text{bpy})_3]^{3+}$, leading to the depletion of the redox mediator [11,14,15]. Consequently, to demonstrate high device stability, most studies limit TBP to moderate concentrations (0.2 M) and use higher concentrations of redox mediators (**Table S1**) [15-18]. In contrast, higher TBP concentrations (0.5 – 1.0 M) are typically used to achieve high PCEs [6,19-21].

In addition to intrinsic degradation, conventional devices, *i.e.*, two electrodes facing each other with an electrolyte in between, suffer from extrinsic degradation. Electrolyte leakage and water ingress are the processes that have the most significant impact on the stability of DSSCs. Water reacts with Co(III) and depletes the oxidized form of the redox mediator [15]. Extrinsic factors can be fully mitigated by air-tight encapsulation [22]. Nevertheless, conventional devices show only a modest improvement in stability; their operational lifetime increases from 200 hours in polymer-encapsulated cells to 800 hours in hermetic-sealed counterparts [23]. Addressing internal degradation factors in high-PCE devices remains a challenging task.

In this study, we conclude that most of the internal degradation factors are mitigated using a monolithic device architecture (M-DSSCs) [23,24] with a carbon counter electrode. The carbon counter electrode effectively suppresses two major photoinduced degradation pathways: the coordination of $[\text{Co}(\text{bpy})_3]^{3+}$ with TBP and its reaction with water. The prepared M-DSSCs show impressive stability even in non-hermetically encapsulated cells. The impact of the device architecture and the porous carbon counter electrode on the PCE degradation pathways was investigated, rendering devices stable for 1000 h under accelerated light soaking.

2. Experimental

2.1. Preparation of DSSCs

Conventional and monolithic structures were prepared as described elsewhere [23]. FTO-coated glass (2.2 mm, TEC7, GreatCell Solar) was used as the photoelectrode (PE) and counter-electrode (CE) substrates; bare soda-lime glass (2 mm, SGG PLANICLEAR, Saint-Gobain) served as

the cover in M-DSSCs. Electrolyte injection holes were drilled in the CE and cover substrates; PE substrates of M-DSSCs were scribed using a 355 nm ns pulse laser. All substrates were washed with detergent and distilled water and treated with air plasma (Diener Electronics) for 10 minutes.

A compact TiO₂ layer was deposited in the PE substrates by spray pyrolysis using a precursor solution consisting of titanium diisopropoxide bis(acetylacetonate) (75 wt.% in isopropanol, Sigma-Aldrich®) in anhydrous 2-propanol. Spray deposition was performed at 450 °C followed by sintering for 45 min. A *ca.* 7 µm transparent TiO₂ layer (Greatcell Solar, 30NR-D) with an area of 0.25 cm² and a *ca.* 7 µm reflector TiO₂ layer (Greatcell Solar, WER2-O) were deposited sequentially by screen printing and sintered at 500 °C for 1 h. For M-DSSCs, a *ca.* 25 µm carbon layer (Elcocarb B/SP, Solaronix®) was applied on top of the reflector TiO₂ layer by doctor-blade and sintered at 400 °C for 1 h. After the cooldown, the substrates were immersed in a 0.1 mM solution of Y123 dye (Dyename) in *tert*-butanol/acetonitrile (1:1 volume ratio) for 24 hours for conventional devices and 48 hours for monolithic devices. The dye loading in the transparent TiO₂ layer is 95 ± 3 nmol·cm⁻² [25].

The PEDOT:PSS counter electrode (CE) was prepared by sequentially spin-coating an aqueous suspension of PEDOT:PSS (Clevios PH 1000) three times, with 5 vol.% DMSO added; each spin-coating was conducted at 3000 rpm for 45 s, followed by drying at 120 °C for 15 min. The resulting layer had a thickness of *ca.* 300 nm. PEDOT CE without PSS was prepared by electropolymerization from 0.01 M ethylenedioxythiophene (EDOT) + 0.1 M sodium dodecyl sulfate aqueous solution. A current of 0.16 mA·cm² for 175 s was applied to the FTO substrates immersed in this solution [26].

The substrates of conventional DSCCs and M-DSSCs were placed together and bonded with thermoplastic sealant (Meltonix 1170-60, Solaronix®) in a hot press. The devices were filled with acetonitrile (ACN)-based electrolyte consisting of 0.165 M/0.045M Co(II/III) tris(bipyridyl) tetracyanoborate (Eversolar, Co-200, and Co-300), 0.1 M LiClO₄ and various concentrations of TBP (indicated in the text). The injection holes were closed with a microscope glass slide and the thermoplastic sealant.

Symmetric half cells were prepared by sandwiching two CE substrates of PEDOT:PSS or PEDOT and sealing them with thermoplastic film.

2.2. Accelerated aging test

The stability of the devices was evaluated under a simulated light intensity of $1000 \text{ W}\cdot\text{m}^{-2}$ in a closed test chamber (Atlas SUNTEST XLS+) equipped with a Xe-lamp and AM1.5G filter. A 390 nm UV cut-off filter (Solaronix®) was used and the temperature of the black body sensor in the chamber was stabilized at $48 \pm 3 \text{ }^{\circ}\text{C}$. A variable resistance was connected to the devices to keep the potential of the cells close to a maximum power point.

2.3. Characterization

The characteristic photocurrent-potential (*J-V*) curves were recorded using a Zennium (Zahner) electrochemical station at $50 \text{ mV}\cdot\text{s}^{-1}$. The simulated solar light AM1.5G, $100 \text{ mW}\cdot\text{cm}^{-2}$, was provided by an Oriel class ABA LED solar simulator (MiniSol LSH 732; Newport). A mask area of 0.16 cm^2 was used for the M-DSSCs, while the conventional configuration was not masked (cell area of 0.25 cm^2). A set of 3 devices was used for each test condition; the average values and the standard deviations for each set are shown in the tables.

Electrochemical impedance spectroscopy (EIS) measurements of fully assembled devices were performed in the dark in the frequency range of $1 \text{ MHz} - 0.1 \text{ Hz}$, applying a sinusoidal perturbation with an amplitude of 10 mV at 50 mV below open-circuit potential. The EIS of dummy devices was measured at 0 V in the same frequency range. An Autolab electrochemical station (PGSTAT 302 N, Metrohm) was used to collect the EIS spectra. ZView software was used to fit the EIS spectra.

Linear sweeping voltammetry (LSV) was performed using a glassy carbon electrode as the working electrode, a platinum wire as the counter electrode, and Ag/AgNO_3 ($0.01 \text{ M AgNO}_3 + 0.1 \text{ M tetrabutylammonium perchlorate (TBAP)}$ in ACN) as the reference electrode; an Autolab electrochemical station (PGSTAT 302 N, Metrohm) was employed to impose the potential scan rate of $20 \text{ mV}\cdot\text{s}^{-1}$ and to read the resulting current density. The DSSC electrolytes for the LSV study were diluted in a supporting solution of 0.1 M TBAP in ACN.

^1H solution Nuclear Magnetic Resonance (NMR) spectra were recorded on a Bruker Avance 300 (300.13 MHz) spectrometer. CD_3CN was used as the solvent and tetramethylsilane (TMS) as the internal reference; the chemical shifts are expressed in δ (ppm). Electrolyte solutions were prepared in the NMR tube and aged under illumination, except for the solution aged in carbon. The electrolyte solution was aged in a dummy carbon device and extracted for analysis. The aged carbon solution was diluted 1:1 (by volume) in CD_3CN .

Thermal Gravimetric Analysis (TGA) was performed in a NETZSCH STA 449 F3 instrument in the temperature range of 30 °C to 600 °C in a nitrogen atmosphere ($35\text{ mL}\cdot\text{min}^{-1}$) at a heating rate of $10\text{ }^\circ\text{C}\cdot\text{min}^{-1}$.

The absorbance spectra were recorded by a VWR® P9 UV-Visible spectrophotometer using a pair of 10.0 mm path length quartz cuvettes.

3. Results and discussion

3.1. Light stability of cobalt-mediated devices

The optimal concentration of recombination-suppressing additives in the DSSC electrolyte depends on the structure and components of the device. High-performing M-DSSCs use 1.2 M of TBP [20], while the optimal TBP concentration for devices with a conventional configuration has been determined to be 0.8 M [6]. M-DSSCs and conventional cells with 1.2 M of TBP showed a PCE of 7.3 % and 8.5 %, respectively (**Tables S2 and S3**). The higher PCE of conventional devices is due to the considerably higher current density. Monolithic and conventional cells with 0.2 M of TBP exhibited lower PCE values of 6.1 % and 6.9 %, respectively, but exhibited significantly improved stability, which agrees well with prior reports [15-17].

Nevertheless, conventional devices exhibited poor PCE stability under accelerated light aging, either with low or high TBP concentrations (**Figure 1a**).

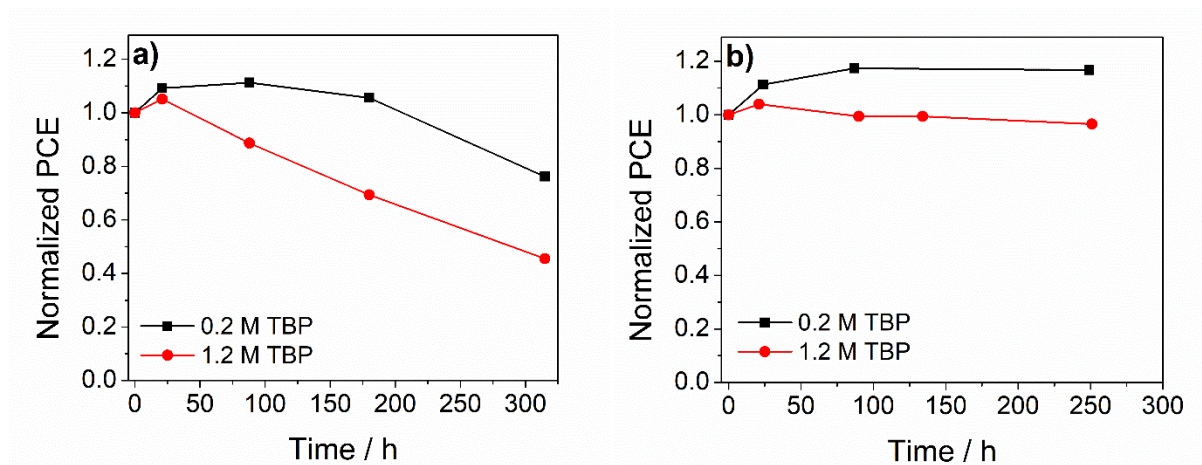


Figure 1 – Normalized PCE during light aging of **(a)** conventional and **(b)** M- DSSCs with 0.2 M and 1.2 M TBP additive in the electrolyte.

After 300 h, the PCE of the cells with 1.2 M and 0.2 M of TBP dropped by 54 % and 24 %, respectively. As expected, cells with higher TBP showed a rapid decrease in photocurrent (**Figure S1**) after 100 h of aging, falling by 37 % after 300 h. The fill factor (FF) showed a significant decrease of 21 %, while the V_{oc} had a minor decay of 8 %. Cells with a lower TBP concentration exhibited reductions in FF and V_{oc} of 18 % and 14 %, respectively, while the short-circuit current density (J_{sc}) increased by 8 %.

In contrast to conventional devices, M-DSSCs exhibited a much more stable PCE history for high and low TBP concentrations (**Figure 1b**). Devices with 1.2 M of TBP showed a minor 3.5 % reduction in PCE. J_{sc} increased by 9.5 %, while the V_{oc} and the FF decreased by 6.3 % and 5.9 %, respectively – **Figure S2**. Monolithic cells with a lower amount of TBP presented outstanding stability, showing a 16.6 % increase in PCE. They exhibited a significant improvement of 21.7 % in J_{sc} and small reductions of 2.2 % and 1.9 % in V_{oc} and FF, respectively (**Figure S2**). Light-soaking increases the J_{sc} by lowering the conduction band of TiO_2 and enhancing the electron injection rate with marginal potential loss [27]. The light-induced current increase has been associated with the interaction between $[Co(bpy)_3]^{3+}$ and TBP, which enhances the charge transfer and ion diffusion at the TiO_2 /electrolyte interface [14]. The improvement in light-induced photocurrent diminishes for higher initial TBP concentrations in both device structures. Notably, M-DSSCs with 0.2 M of TBP exhibited exceptional stability over 1000 hours, with a 7.2 % increase in photovoltaic

performance. It is important to emphasize that these devices were encapsulated using a thermoplastic sealant, which does not provide a hermetic encapsulation, leading to electrolyte leakage and water ingress [22,28].

3.2. Impedance characterization of light-aged devices

The charge transfer resistances in conventional devices during light aging were determined by EIS study (**Figure 2**).

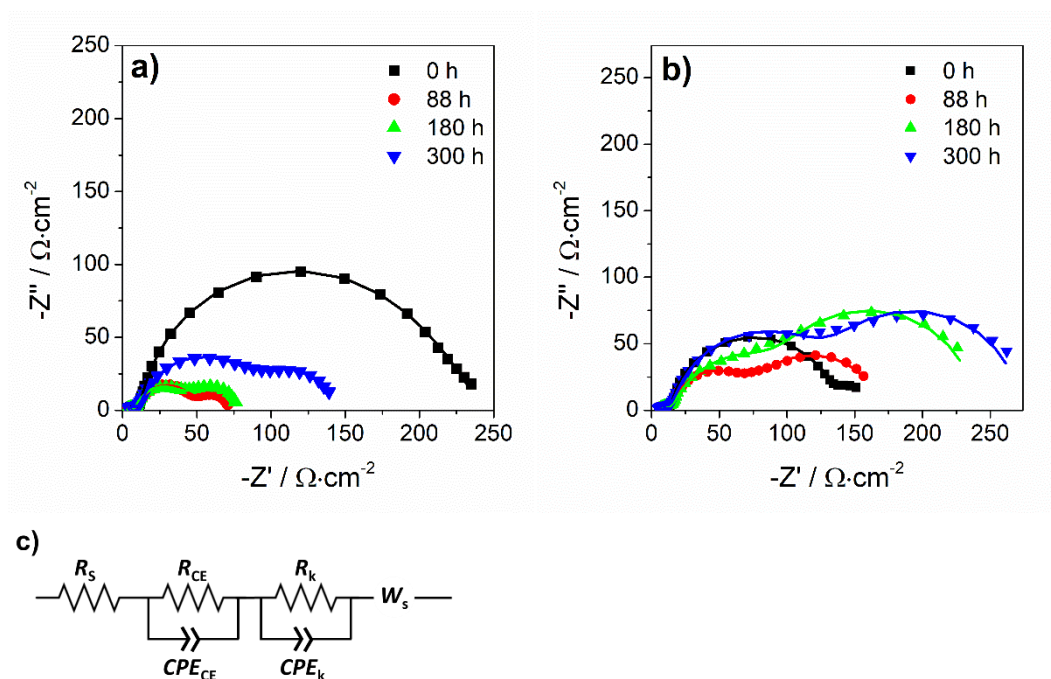


Figure 2 – Nyquist diagrams of conventional DSSC aged under light with cobalt electrolyte containing (a) 0.2 M TBP and (b) 1.2 M TBP; (c) equivalent electrical circuit used to fit the EIS data. Solid lines in plots (a) and (b) represent fittings.

An equivalent electric circuit (**Figure 2c**) was fitted the EIS plots. R_s represents the series resistance; R_{CE} and R_k denote the charge transfer resistances at the CE and recombination resistance at the PA, respectively. CPE_{CE} and CPE_k are the respective constant phase elements. W_s is a short Warburg element for finite-length diffusion with resistance R_d . The values of the resistances obtained by fitting are summarized in **Table 1**.

Table 1 –Internal resistances ($\Omega\cdot\text{cm}^2$) of conventional DSSC with cobalt electrolyte containing 0.2 M TBP and 1.2 M TBP.

Aging time / h	0.2 M TBP				1.2 M TBP			
	R_s	R_{CE}	R_k	R_d	R_s	R_{CE}	R_k	R_d
0	3.0	6.8	186.5	43.0	3.1	11.7	115.6	30.2
88	2.5	7.0	32.1	31.1	3.8	8.3	39.9	117.3
180	2.8	5.0	25.9	43.8	3.9	8.8	46.5	179.9
300	2.9	6.9	62.4	71.4	3.4	8.9	83.6	175.9

During the first hours of light soaking, R_k decreases in devices with 0.2 M and 1.2 M TBP. Under illumination and load, the dye is excited, and electrons are injected into the conduction band of the TiO_2 . The oxidized dye is then regenerated by $[\text{Co}(\text{bpy})_3]^{2+}$, which oxidizes, forming $[\text{Co}(\text{bpy})_3]^{3+}$. This increases the concentration of $[\text{Co}(\text{bpy})_3]^{3+}$ at the TiO_2 /electrolyte interface, promoting electron recombination, as observed by the decrease in R_k . At the end of the test, R_k increased twofold compared to the values at 88 hours for both concentrations of TBP. However, R_k was higher for 1.2 M TBP devices, reaching $83.6 \Omega\cdot\text{cm}^2$ compared to $62.4 \Omega\cdot\text{cm}^2$ for 0.2 M TBP cells.

The R_d in cells with 0.2 M TBP was initially slightly lower than in the counterparts with 1.2 M TBP; R_d increased from $43 \Omega\cdot\text{cm}^2$ to $71 \Omega\cdot\text{cm}^2$ after 300 h of aging. Cells with higher TBP concentrations exhibited a significant increase in R_d from $30 \Omega\cdot\text{cm}^2$ to $176 \Omega\cdot\text{cm}^2$. The higher R_d correlates well with the decrease in PCE during light aging (**Figure 1a**).

As the EIS spectra were recorded in the dark, no photoelectrons were generated, and the dominant reaction at the photoanode is the electron transfer from the TiO_2 layer to $[\text{Co}(\text{bpy})_3]^{3+}$. The reduced mediator $[\text{Co}(\text{bpy})_3]^{2+}$ is formed and diffuses to the CE, where it is oxidated to $[\text{Co}(\text{bpy})_3]^{3+}$ and then diffuses back to the TiO_2 layer [29]. The increase in R_d indicates a decrease in the concentration of the $[\text{Co}(\text{bpy})_3]^{3+}$ species in the aged devices, which is more pronounced at higher TBP concentrations. The R_d is inversely related to the concentration and diffusion coefficient of the redox mediators [29]. The initial concentration of $[\text{Co}(\text{bpy})_3]^{3+}$ in the electrolyte formulation is *ca.* 3.7 times lower than that of $[\text{Co}(\text{bpy})_3]^{2+}$; $[\text{Co}(\text{bpy})_3]^{3+}$ limits the electrolyte diffusion resistance. The diffusion coefficients of $[\text{Co}(\text{bpy})_3]^{2+}$ and $[\text{Co}(\text{bpy})_3]^{3+}$ are similar and do not vary significantly during the aging process [30,31]. The reduction in the concentration of $[\text{Co}(\text{bpy})_3]^{3+}$ affects the R_k ; the lower concentration of $[\text{Co}(\text{bpy})_3]^{3+}$ species at the TiO_2 /electrolyte

interface results in lower electron recombination and consequently higher R_k (**Table 1**). The R_{CE} at the CE/electrolyte interface remained almost unchanged, indicating that the catalytic activity of the PEDOT:PSS layer is not affected by aging.

The effect of TBP concentration on light-induced electrolyte degradation was analyzed from the current-potential response of symmetrical dummy cells with PEDOT:PSS (**Figure 3**). The current density in the dummy cells with 1.2 M TBP (**Figure 3a**) exhibited a continuous reduction. After 241 hours, the characteristic J - V curve was no longer visible and the diffusion limiting current was nearly zero. This indicates that almost no $[\text{Co}(\text{bpy})_3]^{3+}$ was present in the electrolyte after light soaking. The decrease in current density was less pronounced for the 0.2 M TBP (**Figure 3b**). After 476 h, the limiting current was reduced by half. The J - V curves of the dummy cells with 0.2 M TBP stored in the dark (**Figure S3**) remained unchanged after 476 hours. In contrast, the J - V curves of dummy devices with 1.2 M TBP showed a slight decrease in current over the same period.

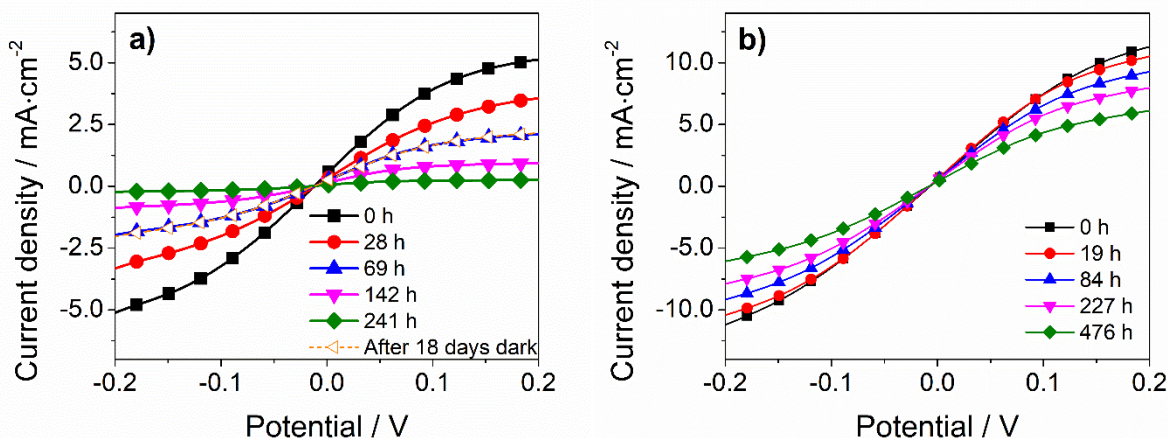


Figure 3 – Current-potential curves of light-aged symmetric dummy cells with PEDOT:PSS and cobalt electrolyte containing (a) 1.2 M TBP and (b) 0.2 M TBP.

The reduction in the current density in the dummy cells was attributed to the loss of redox mediators, which is consistent with the EIS response of the dummy cells shown in **Figures S4** and **S5**. The resistances R_s , R_{CE} , and R_d of the dummy cells (**Table 2**) were obtained by fitting the equivalent circuit model to the EIS spectra – **Figure S6**. For 1.2 M dummy cells, R_d increased twentyfold, from $15.2 \Omega \cdot \text{cm}^2$ to $319.6 \Omega \cdot \text{cm}^2$, whereas for 0.2 M dummy cells, the increase was only twofold, from $8.6 \Omega \cdot \text{cm}^2$ to $19.5 \Omega \cdot \text{cm}^2$. For higher TBP concentration, R_d increased more

significantly, indicating a higher loss of charge carriers in the electrolyte. As reported [13], $[\text{Co}(\text{bpy})_3]^{3+}$ interacts with TBP to form a TBP-shielded $[\text{Co}(\text{bpy})_3]^{3+}$ complex. The formation of the $[\text{Co}(\text{bpy})_3]^{3+}$ -TBP complex is facilitated by prolonged light exposure and by higher concentration of TBP molecules in solution [15]. Electrolytes with a higher TBP/ $[\text{Co}(\text{bpy})_3]^{3+}$ ratio show faster degradation due to $[\text{Co}(\text{bpy})_3]^{3+}$ -TBP complexation under light exposure, as observed for light-aged dummy devices. When kept in the dark, only dummy devices with high TBP concentrations show a slight increase in R_d . This suggests that $[\text{Co}(\text{bpy})_3]^{3+}$ -TBP complexation is thermodynamically favorable and occurs naturally, albeit quite slowly. It can then be concluded that the reaction between $[\text{Co}(\text{bpy})_3]^{3+}$ and TBP reduces the concentration of active and mobile $[\text{Co}(\text{bpy})_3]^{3+}$ ions, resulting in higher electrolyte diffusion resistances.

The significant increase in R_{CE} observed in cells containing 1.2 M TBP can be attributed to one of the two factors: i) limited availability of pristine $[\text{Co}(\text{bpy})_3]^{3+}$ ions at the PEDOT:PSS/electrolyte interface; ii) loss of electrocatalytic activity of the PEDOT:PSS film. The latter factor was eliminated based on the following considerations. Previous studies [16] showed that electropolymerized PEDOT CE fully retains its catalytic activity during aging with cobalt electrolytes. In support of this, the J - V curves of dummy cells with electropolymerized PEDOT (**Figure S7**) showed the same trend of current loss as the PEDOT:PSS counterparts (**Figure 3a**). Specifically, the current density in both types of cells decreased continuously to almost zero during light aging, while devices stored in the dark exhibited only minor reductions in current. These observations indicate that the PEDOT:PSS maintains its electrocatalytic activity under light aging conditions; the increase in R_{CE} is mainly due to the depletion of pristine $[\text{Co}(\text{bpy})_3]^{3+}$.

Table 2 – Resistances in $\Omega \cdot \text{cm}^2$ of dummy cells with cobalt electrolyte containing 0.2 M TBP and 1.2 M TBP. Cells were aged under light and in the dark.

TBP	Aging time / h	R_s		R_{CE}		R_d	
		Light	Dark	Light	Dark	Light	Dark
1.2 M	0	1.2	1.3	3.9	5.0	15.2	16.0
	28	1.3	1.3	7.2	6.7	23.6	18.1
	69	1.4	1.3	9.4	7.9	37.0	19.7
	142	1.5	1.3	14.9	8.6	77.8	20.1
	241	1.6	1.3	35.9	10.1	293.2	24.5
	18 days dark	1.4	---	10.4	---	35.8	---
0.2 M	0	1.2	1.4	2.3	2.0	8.6	9.8

19	1.2	1.2	2.9	2.2	10.3	9.9
84	1.5	1.2	3.7	2.4	11.4	10.1
227	1.1	1.2	4.1	2.5	14.1	10.2
476	1.2	1.2	5.4	2.9	19.5	11.0

Interestingly, dummy cells with 1.2 M TBP, which underwent light aging and were subsequently stored in the dark for 18 days, showed a partial recovery of the current density and the J - V characteristic (**Figure 3a**). A similar recovery was observed for the cells with electropolymerized PEDOT (**Figure S7**). This suggests that the interaction between TBP and $[\text{Co}(\text{bpy})_3]^{3+}$ is reversible. Impedance analysis shows a “recovery” of R_d and R_{CE} after the dark storage period (**Table 2**). R_d and R_{CE} decreased significantly from $319.6 \Omega \cdot \text{cm}^2$ and $28.9 \Omega \cdot \text{cm}^2$ to $35.8 \Omega \cdot \text{cm}^2$ and $10.4 \Omega \cdot \text{cm}^2$, respectively. The reduction in both resistances is evidence of pristine electroactive and that mobile $[\text{Co}(\text{bpy})_3]^{3+}$ ions are available in the electrolyte, albeit at a lower concentration than in the initial solution.

3.3. Electrochemical characterization of $[\text{Co}(\text{bpy})_3]^{3+}$ /TBP electrolytes

The light-induced loss of active $[\text{Co}(\text{bpy})_3]^{3+}$ species in the electrolyte in the presence of TBP was confirmed by LSV (**Figure 4**). LSV curves were recorded for electrolytes consisting of 0.165 M/0.045 M $[\text{Co}(\text{bpy})_3]^{2+/3+}$, 0.1 M LiClO_4 and TBP concentrations of 1.2 M, 0.58 M, 0.2 M, and 0.045 M. Measurements were performed for freshly prepared electrolytes and aged electrolytes under light soaking for 225 h. The maximum peak currents associated with oxidation of $[\text{Co}(\text{bpy})_3]^{2+}$ and reduction of $[\text{Co}(\text{bpy})_3]^{3+}$ ions are shown in **Table S4**. All LSVs of light-aged electrolytes exhibited a peak current reduction associated with both cobalt redox complexes.

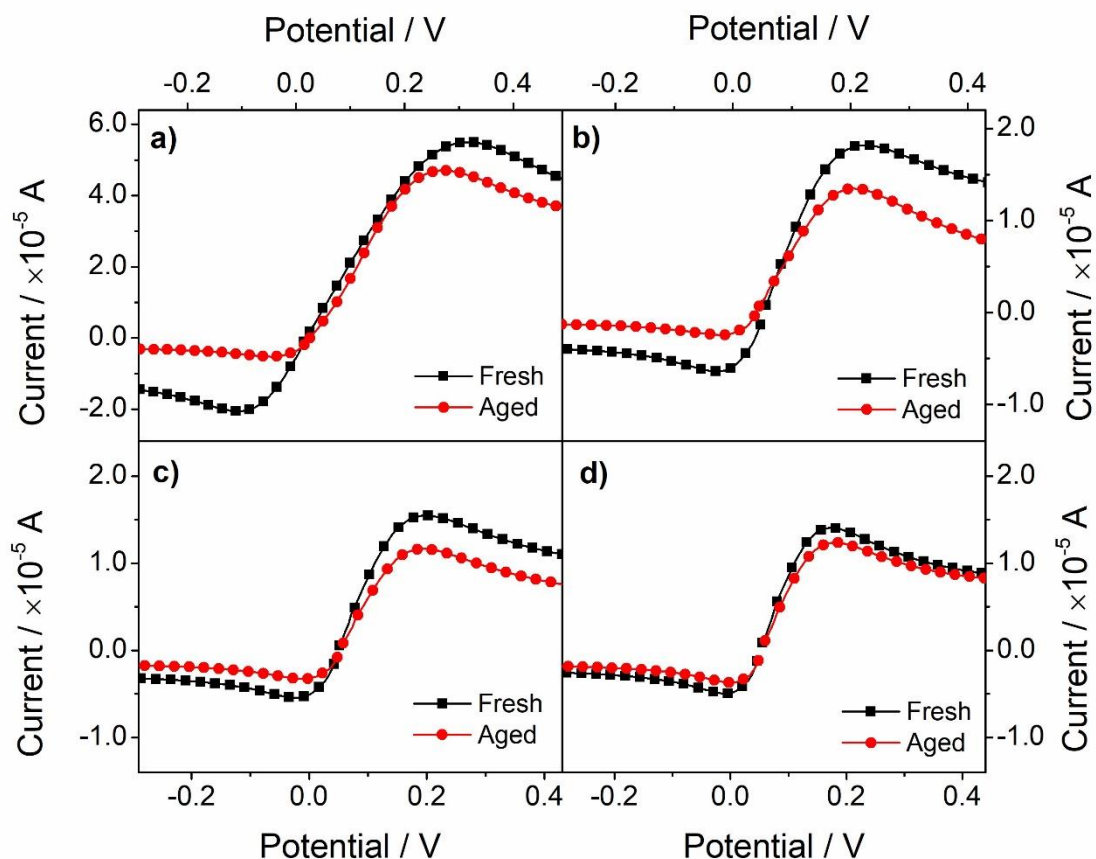


Figure 4 – LSV curves recorded in electrolytes: 0.165 M/0.045 M $[\text{Co}(\text{bpy})_3]^{2+/3+}$, 0.1 M LiClO_4 with (a) 1.2 M, (b) 0.58 M, (c) 0.2 M and (d) 0.045 M TBP before and after light aging for 225 h; 1.25% (v/v) electrolyte solution in ACN with 0.1 M TBAP.

As illustrated in **Figure 4** and detailed **Table 3**, the decrease in $[\text{Co}(\text{bpy})_3]^{3+}$ concentration was more pronounced in electrolytes with higher TBP concentrations. **Table 3** presents the aged/initial and $[\text{Co}(\text{bpy})_3]^{2+/3+}$ peak current ratios, highlighting that the electrolyte with 1.2 M TBP exhibits the highest increase in the $[\text{Co}(\text{bpy})_3]^{2+/3+}$ current ratio from 2.7 to 8.9. Electrolytes with 0.58 M, 0.2 M, and 0.045 M TBP show progressively lower aged $[\text{Co}(\text{bpy})_3]^{2+/3+}$ current ratios of 5.5, 3.9, and 3.2, respectively. This trend indicates a clear loss of active $[\text{Co}(\text{bpy})_3]^{3+}$ ions, as evidenced by the aged/initial ratio for each cobalt mediator. Notably, the aged/initial ratio of $[\text{Co}(\text{bpy})_3]^{2+}$ is similar for all electrolytes, whereas the aged/initial ratio of $[\text{Co}(\text{bpy})_3]^{3+}$ decreases with increasing TBP in the electrolyte.

Table 3 – Ratio of the maximum peak current obtained from the LSV curves in electrolytes with different TBP concentrations. Cells were aged under light for 225 h.

TBP / M	Initial Co(II)/Co(III)	Aged Co(II)/Co(III)	Co(II) Aged/Initial	Co(III) Aged/Initial
1.2	2.7	8.9	0.85	0.26
0.58	2.8	5.5	0.75	0.38
0.2	2.8	3.9	0.82	0.60
0.045	2.9	3.2	0.85	0.75

The LSV curves of aged electrolytes were recorded over a broader range of potentials to detect the formation or complexation of different cobalt complexes. The peak associated with the $[\text{Co}(\text{bpy})_3]^{3+}$ disappears after 330 h of aging (**Figure 5a**), and a secondary peak emerges at more negative potentials. This peak is potentially attributable to a $[\text{Co}(\text{bpy})_3]^{3+}$ -TBP complex, which is not present in the fresh electrolyte. An analogous disappearance of the $[\text{Co}(\text{bpy})_3]^{3+}$ peak and the appearance of a secondary peak at a more negative potential was observed for the aged electrolytes prepared only with $[\text{Co}(\text{bpy})_3]^{3+}$ ions (**Figure 5b**). After storage in the dark for 7 days, the secondary peak shifted towards more negative potential or diminished. This observation may indicate the dissociation of the $[\text{Co}(\text{bpy})_3]^{3+}$ -TBP complex and subsequent recovery of the $[\text{Co}(\text{bpy})_3]^{3+}$ mediator, as previously observed in dummy cells.

The aged electrolyte containing solely the $[\text{Co}(\text{bpy})_3]^{3+}$ mediator shows a peak at a positive potential associated with the $[\text{Co}(\text{bpy})_3]^{2+}$ mediator (**Figure 5b**). The formation of $[\text{Co}(\text{bpy})_3]^{2+}$ is likely due to the reaction of $[\text{Co}(\text{bpy})_3]^{3+}$, TBP, and water.[30] The ingress and presence of water in the electrolyte are related to the use of a water-permeable polymer for encapsulation and to the presence of water in the reagents. These findings suggest that two reactions occur during light aging, leading to the loss of the $[\text{Co}(\text{bpy})_3]^{3+}$ mediator. i) $[\text{Co}(\text{bpy})_3]^{3+}$ interacts with TBP to form a complex that does not participate in the redox reaction during cell operation, and ii) $[\text{Co}(\text{bpy})_3]^{3+}$ is converted to $[\text{Co}(\text{bpy})_3]^{2+}$ by a reaction with TBP and water.

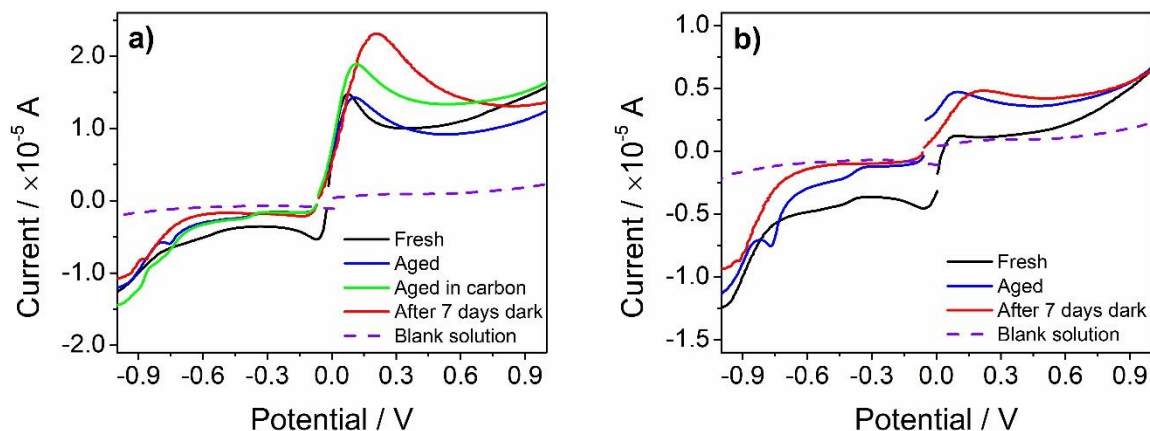


Figure 5 – Linear sweep voltammetry of electrolyte solution containing 1.2 M TBP, 0.1 LiClO₄ and **(a)** 0.165 M/0.045 M [Co(bpy)₃]^{2+/3+} and **(b)** only 0.045 M [Co(bpy)₃]³⁺ before and after 330 h of light aging; 1.25% (v/v) electrolyte solution in ACN with 0.1 M TBAP.

In monolithic devices, the cell consists of multiple stacked mesoporous layers, with the uppermost layer being carbon. The high surface area of the carbon promotes the adsorption of TBP, reducing the number of free TBP available in solution to coordinate with the [Co(bpy)₃]³⁺. Additionally, the opacity of the carbon blocks light, preventing light-induced reactions, and its hydrophobic nature might prevent some water molecules from ingress into the mesoporous stack [32]. For these reasons, the carbon layer was expected to minimize the factors affecting the loss of [Co(bpy)₃]³⁺. However, electrolytes aged in contact with the carbon layer exhibit a similar decrease in the [Co(bpy)₃]³⁺ reduction peak, as shown in **Figure 5a**. In the presence of carbon, the secondary peak observed at a more negative potential of *ca.* -0.75 V is less evident; the LSV curve does not have a distinct peak. This behavior indicates that the formation of the [Co(bpy)₃]³⁺-TBP complex is smaller in the aged electrolyte when carbon is present, likely due to the reduced concentration of active TBP absorbed by the carbon. Despite this, electrolyte degradation still occurs with the carbon CE, primarily due to the loss of [Co(bpy)₃]³⁺ mediator, either through its conversion to [Co(bpy)₃]³⁺-TBP complex or its reduction to [Co(bpy)₃]²⁺.

At this point, it is essential to highlight the practical differences when analyzing electrolyte samples from conventional and monolithic cells, which use a thin PEDOT:PSS layer (*ca.* 0.3 μm) and a thick mesoporous organophilic carbon layer (*ca.* 30 μm) as counter-electrodes, respectively. The high porosity, high thickness, and organophilic nature of carbon counter-

electrode retain most of the electrolyte within its porous structure, making it challenging to extract a sample. As a result, most of the electrolyte collected from carbon-based monolithic cells originate from the free volume surrounding the porous structure of the cell. In contrast, in conventional PEDOT:PSS devices, the electrolyte is in free space, making it easy to collect a sample. This fundamental difference affects how electrolyte samples are obtained and analyzed from each cell type.

3.4. Spectroscopic characterization of $[\text{Co}(\text{bpy})_3]^{3+}$ /TBP electrolytes

To further investigate the complexation and chemical transformations between $[\text{Co}(\text{bpy})_3]^{3+}$ and TBP, NMR analyses were performed (**Figures 6 and S8-S12**). The spectra of light-aged electrolyte solutions containing $[\text{Co}(\text{bpy})_3]^{3+}$ /TBP mixture show significant changes as the light-soaking time increases.

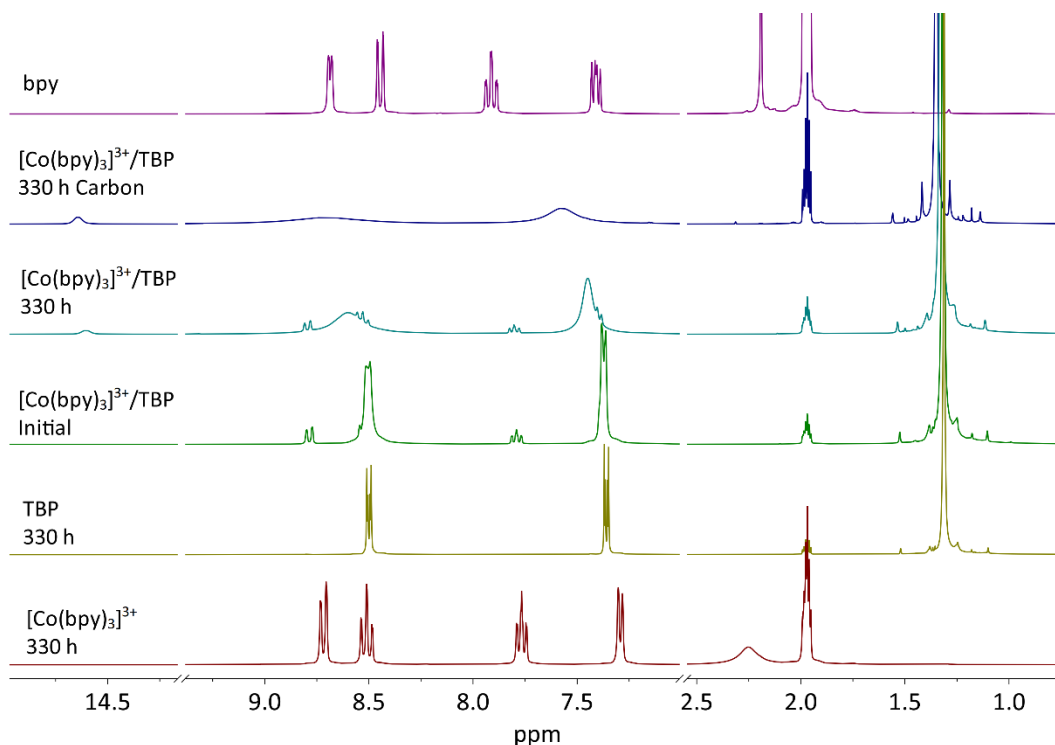


Figure 6 – ^1H NMR spectra of $[\text{Co}(\text{bpy})_3]^{3+}$ /TBP solution recorded before and after light aging, as well as of light-aged $[\text{Co}(\text{bpy})_3]^{3+}$ and TBP solutions in CDCl_3 . The ^1H NMR spectrum of bipyridine (bpy) is shown for comparison. The concentrations of $[\text{Co}(\text{bpy})_3]^{3+}$ and TBP/bpy used were 0.045 M and 1.2 M, respectively.

After exposure to light, a new signal appears at δ 14.6 ppm (**Figures 6 and S12**), which has been attributed to a different paramagnetic cobalt complex [30]. This peak is absent in light-aged solutions containing only $[\text{Co}(\text{bpy})_3]^{3+}$ complex (**Figure S8**) or only TBP (**Figure S9**). Both species ($[\text{Co}(\text{bpy})_3]^{3+}$ and TBP) remain stable when present alone in the solution. However, when mixed, they readily interact – **Figure 6**. The signal at δ 7.29 ppm from $[\text{Co}(\text{bpy})_3]^{3+}$ downshifts and overlaps with the TBP signal, which shifts from δ 7.36 ppm to δ 7.37 ppm. This overlapping might result from the shielding effect of the TBP in the presence of the $[\text{Co}(\text{bpy})_3]^{3+}$ mediator [13]. As the $[\text{Co}(\text{bpy})_3]^{3+}$ /TBP solution ages under light, all NMR signals undergo a downshift – **Figures S11 and S12**. The TBP peaks shift significantly from δ 7.37 ppm and δ 8.51 ppm to δ 7.45 ppm and δ 8.60 ppm, respectively, becoming broader. According to Gao *et al.* [30], these changes, along with the appearance of the δ 14.6 ppm signal, are indicative of a photoinduced reaction between $[\text{Co}(\text{bpy})_3]^{3+}$ and TBP in the presence of water. This reaction is assumed to form a paramagnetic Co(II) complex with a seven-coordination geometry and protonated TBP (TBP-H^+ or TBP-OH^-). Protonation induces the downshift observed in the TBP signal [33]. Additionally, the formation of a N-H bond in TBP can also be attributed to the chemical shift observed at δ 14.6 ppm [34]. The water signal is detected and shifts from δ 3.1 ppm in the initial $[\text{Co}(\text{bpy})_3]^{3+}$ /TBP solution to δ 3.6 ppm after 100 h and to δ 4.4 ppm after 330 h of light aging. This reaction causes the decrease in $[\text{Co}(\text{bpy})_3]^{3+}$ signal and an increase in the intensity of the peak at δ 14.6 ppm with light exposure, as observed in **Figures S10 and S12**.

Light aging of the $[\text{Co}(\text{bpy})_3]^{3+}$ /TBP solution within the carbon layer was expected to slow the $[\text{Co}(\text{bpy})_3]^{3+}$ /TBP interaction primarily due to the optical opacity of the carbon layer and the adsorption of TBP onto its surface. However, as shown in **Figure 6**, the NMR spectrum indicates the opposite behavior. This should be evaluated considering the peculiarities of electrolyte extraction from the carbon layer (as noted above) and other contributing factors. As observed for aged electrolyte solutions without carbon, the TBP signals at δ 7.37 ppm and δ 8.51 ppm downshift to δ 7.57 ppm and δ 8.70 ppm, respectively, and become broader. Meanwhile, the signals associated with the $[\text{Co}(\text{bpy})_3]^{3+}$ mediator between δ 7 ppm and δ 9 ppm disappear, suggesting a higher reaction rate between $[\text{Co}(\text{bpy})_3]^{3+}$ and TBP in the presence of a carbon. This results in a reduction of cobalt species and an increase in protonated TBP. Indeed, the presence

and highest intensity of the peak at δ 14.64 ppm support this assumption. Additionally, the water signal is present at δ 3.37 ppm, arising from both initial cobalt salts and solvents in the electrolyte and water-permeable polymeric encapsulation. As evidence, the water signal is detected in the NMR spectra of both $[\text{Co}(\text{bpy})_3]^{3+}$ (**Figure S8**) and TBP (**Figure S9**) at δ 2.2 ppm and δ 2.8 ppm, respectively.

Overall, NMR spectra of aged electrolytes around the carbon layer suggest a faster interaction of $[\text{Co}(\text{bpy})_3]^{3+}$ with TBP, leading to increased electrolyte deterioration. However, when integrated into a monolithic architecture, cobalt-mediated DSSCs exhibit stable performance under continuous light soaking (**Figure 1**). The apparent discrepancy between the dynamic NMR spectra and the stability of the M-DSSCs suggests that different electrolyte deterioration phenomena occur outside and inside the porous carbon layer. In the surrounding area, the electrolyte is exposed to light, allowing $[\text{Co}(\text{bpy})_3]^{3+}$ ions and TBP to interact freely, like the free-moving electrolyte between electrodes in the conventional structure.

Inside the porous carbon, the electrolyte is trapped, significantly slowing ionic diffusion. This phenomenon is supported by TGA (**Figure S13**), which shows a characteristic temperature-induced mass loss for the cobalt complex observed after being in contact with the electrolyte. Additionally, the availability of active TBP molecules for interaction with $[\text{Co}(\text{bpy})_3]^{3+}$ is reduced within the carbon layer due to TBP adsorption [35]. The quantity of TBP adsorbed by the carbon was determined using UV-Vis absorbance spectroscopy (**Figure S14**) and the Beer-Lambert Law: $A_{\text{Abs}} = \varepsilon \cdot c \cdot \ell$ where A_{Abs} is the absorbance, ε is the molar extinction coefficient, c is the concentration, and ℓ is the light path length (see Supporting Information). In the measured solution, the TBP concentration decreased from 1.2 M to 1.087 M, indicating an adsorption of *ca.* 0.69 mmol of TBP per gram of carbon. The reduced ionic diffusion, the TBP adsorption, and the optical opacity of carbon suppress the photoinduced coordination and redox interaction between $[\text{Co}(\text{bpy})_3]^{3+}$, TBP, and water. This is reflected in the exceptional stability of polymer-sealed M-DSSCs (**Figure S2**). Although the electrolyte leaked from the surrounding area of the cell stack (**Figure S15**), the devices continued to operate because the electrolyte was retained within the porous structure. The impressive stability of the photovoltaic metrics in devices with leakage was monitored for more than 1000 h. Despite typically presenting slightly lower PCE than

conventional configurations, monolithic DSSCs offer significantly enhanced stability, positioning them as the most viable option for real-world deployment.

Looking ahead, further research is needed to clarify how Co(II/III) redox mediators and TBP interact within the porous carbon and how these interactions impact long-term PV performance. Characterizing the molecular structure of the $[\text{Co}(\text{bpy})_3]^{3+}$ -TBP complex and its redox properties will provide valuable insights into electrolyte-carbon interfaces. This understanding could guide strategies to enhance the operational stability of other types of monolithic DSSCs.

4. Conclusions

The long-term stability of cobalt-mediated DSSCs is significantly influenced by the electrolyte composition and, more notably, the device architecture. This study demonstrates that monolithic DSSCs with highly porous carbon CE offer superior operational stability compared to conventional counterparts. The light-induced degradation of cobalt electrolytes is primarily attributed to two photoinduced mechanisms: TBP shielding/coordination with $[\text{Co}(\text{bpy})_3]^{3+}$ and redox reaction of $[\text{Co}(\text{bpy})_3]^{3+}$, TBP, and water. These degradation mechanisms were found to contribute to the reduction of $[\text{Co}(\text{bpy})_3]^{3+}$ concentration and a decline in photovoltaic performance in conventional devices.

In contrast, the porous and opaque carbon counter electrode of M-DSSC restricts the electrolyte components, effectively suppressing the detrimental light-induced interactions between $[\text{Co}(\text{bpy})_3]^{3+}$ and TBP. The high surface area of carbon further slows the degradation processes by adsorbing TBP. These findings highlight the intricate interplay between TBP concentration, electrolyte degradation mechanisms, and device stability. Remarkably, 1000 h of complete operational stability under light soaking aging was achieved even in non-hermetically encapsulated devices. The monolithic structure, combined with optimized electrolyte composition and hermetic encapsulation, presents a promising pathway toward developing highly stable DSSCs for practical applications.

Authorship contribution statement

Jorge Martins: Investigation, Methodology, Conceptualization, Formal analysis, Data curation, Writing – original draft. **Ana M.V.M. Pereira:** Investigation, Formal analysis, Writing – original draft. **Seyedali Emami:** Writing – original draft, Writing – review & editing. **Carlos Manuel Silva:** Writing – review & editing. **Dzmitry Ivanou:** Investigation, Supervision, Data curation, Writing – original draft. **Adélio Mendes:** Funding acquisition, Supervision, Investigation, Writing – original draft.

Declaration of Competing Interest

The authors declare that they have no known competing financial interests or personal relationships that could have appeared to influence the work reported in this paper.

Acknowledgements

Jorge Martins is grateful to the Portuguese Foundation for Science and Technology (FCT) for his PhD grant (SFRH/BD/147201/2019). This work was financially supported by: (i) LA/P/0045/2020 (ALICE), UIDB/00511/2020, and UIDP/00511/2020 (LEPABE), funded by national funds through FCT/MCTES (PIDDAC); (ii) project TanPT (2022.05826.PTDC), funded by FEDER funds through COMPETE2020 – Programa Operacional Competitividade e Internacionalização (POCI) and by national funds (PIDDAC) through FCT/ MCTES; (iii) project Diamond funded by the European Union’s Horizon Europe Framework Programme for research and innovation Programme under the grant agreement no. 101084124; (iv) Alliance for Energy Transition (ATE) no. C644914747-00000023, project 56 of the Incentive System “Agendas for Business Innovation”, financed by the Recovery and Resilience Plan (PRR) and by European Funds NextGeneration EU; (v) CICECO – Aveiro Institute of Materials, UIDB/50011/2020, UIDP/50011/2020 & LA/P/0006/2020, financed by national funds through the FCT/MCTES (PIDDAC); and (vi) the Portuguese NMR Network – “The NMR spectrometers are part of the National NMR Network (PTNMR) and partially supported by Infrastructure Project N^o 022161 (co-financed by FEDER through COMPETE 2020, POCI and PORL and FCT through PIDDAC)”.

References

- [1] A. B. Muñoz-García, I. Benesperi, G. Boschloo, J. J. Concepcion, J. H. Delcamp, E. A. Gibson, G. J. Meyer, M. Pavone, H. Pettersson, A. Hagfeldt, M. Freitag, Dye-sensitized solar cells strike back. *Chemical Society Reviews* 50(22) (2021) 12450-12550, 10.1039/D0CS01336F
- [2] X. Huang, Y. Gao, W. Li, J. Wang, G. Yue, F. Tan, H.-L. Wang, Efficient and Stable Z907-Based Dye-Sensitized Solar Cells Enabled by Suppressed Charge Recombination and Photocatalytic Activity. *ACS Sustainable Chemistry & Engineering* 12(34) (2024) 13007-13016, 10.1021/acssuschemeng.4c05171
- [3] Masud, H. K. Kim, Redox Shuttle-Based Electrolytes for Dye-Sensitized Solar Cells: Comprehensive Guidance, Recent Progress, and Future Perspective. *ACS Omega* 8(7) (2023) 6139-6163, 10.1021/acsomega.2c06843
- [4] S. C. Pradhan, A. Hagfeldt, S. Soman, Resurgence of DSCs with copper electrolyte: a detailed investigation of interfacial charge dynamics with cobalt and iodine based electrolytes. *Journal of Materials Chemistry A* 6(44) (2018) 22204-22214, 10.1039/c8ta06948d
- [5] J. Wu, Z. Lan, J. Lin, M. Huang, Y. Huang, L. Fan, G. Luo, Electrolytes in Dye-Sensitized Solar Cells. *Chemical Reviews* 115(5) (2015) 2136-2173, 10.1021/cr400675m
- [6] A. Yella, H.-W. Lee, H. N. Tsao, C. Yi, A. K. Chandiran, M. K. Nazeeruddin, E. W.-G. Diao, C.-Y. Yeh, S. M. Zakeeruddin, M. Grätzel, Porphyrin-Sensitized Solar Cells with Cobalt (II/III)-Based Redox Electrolyte Exceed 12 Percent Efficiency. *Science* 334(6056) (2011) 629-634, 10.1126/science.1209688
- [7] H. R. Zhou, M. Aftabuzzaman, Masud, S. H. Kang, H. K. Kim, Key Materials and Fabrication Strategies for High-Performance Dye-Sensitized Solar Cells: Comprehensive Comparison and Perspective. *Acs Energy Letters* 10(2) (2025) 881-895, 10.1021/acsenenergylett.4c03579
- [8] K. Kakiage, Y. Aoyama, T. Yano, K. Oya, J.-i. Fujisawa, M. Hanaya, Highly-efficient dye-sensitized solar cells with collaborative sensitization by silyl-anchor and carboxy-anchor dyes. *Chemical Communications* 51(88) (2015) 15894-15897, 10.1039/C5CC06759F
- [9] T. Higashino, H. Imahori, Emergence of Copper(I/II) Complexes as Third-Generation Redox Shuttles for Dye-Sensitized Solar Cells. *ACS Energy Letters* 7(6) (2022) 1926-1938, 10.1021/acsenenergylett.2c00716
- [10] F. Bella, S. Galliano, C. Gerbaldi, G. Viscardi, Cobalt-Based Electrolytes for Dye-Sensitized Solar Cells: Recent Advances towards Stable Devices. *Energies* 9(5) (2016) 384, 10.3390/en9050384
- [11] J. Gao, M. Bhagavathi Achari, L. Kloo, Long-term stability for cobalt-based dye-sensitized solar cells obtained by electrolyte optimization. *Chem Commun (Camb)* 50(47) (2014) 6249-6251, 10.1039/c4cc00698d
- [12] T. M. Koh, K. Nonomura, N. Mathews, A. Hagfeldt, M. Grätzel, S. G. Mhaisalkar, A. C. Grimsdale, Influence of 4-tert-Butylpyridine in DSCs with CoII/III Redox Mediator. *The Journal of Physical Chemistry C* 117(30) (2013) 15515-15522, 10.1021/jp403918q
- [13] N. T. Salim, X. Yang, S. Zhang, J. Liu, A. Islam, L. Han, Shielding effects of additives in a cobalt(ii/iii) redox electrolyte: toward higher open-circuit photovoltages in dye-sensitized solar cells. *Journal of Materials Chemistry A* 2(27) (2014) 10532-10539, 10.1039/C4TA01278J
- [14] J. Gao, G. K. Prajapati, Y. Hao, L. Kloo, Exploring Lewis-Base Effects to Improve the Efficiency of [Co(bpy)₃]^{2+/3+}-Mediated Dye-Sensitized Solar Cells. *ACS Applied Energy Materials* 3(6) (2020) 5705-5711, 10.1021/acsaem.0c00665
- [15] J. Gao, A. Tot, H. Tian, J. M. Gardner, D. Phuyal, L. Kloo, Electrochemical impedance and X-ray absorption spectroscopy analyses of degradation in dye-sensitized solar cells containing cobalt tris(bipyridine) redox shuttles. *Physical Chemistry Chemical Physics* 24(31) (2022) 18888-18895, 10.1039/D2CP02283D

- [16] A. Kamppinen, K. Aitola, A. Poskela, K. Miettunen, P. D. Lund, Stability of cobalt complex based dye solar cells with PEDOT and Pt catalysts and different electrolyte concentrations. *Electrochimica Acta* 335 (2020) 135652, 10.1016/j.electacta.2020.135652
- [17] W. Yang, Y. Hao, P. Ghamgosar, G. Boschloo, Thermal Stability Study of Dye-Sensitized Solar Cells with Cobalt Bipyridyl-based Electrolytes. *Electrochimica Acta* 213 (2016) 879-886, 10.1016/j.electacta.2016.07.112
- [18] J. Gao, W. Yang, M. Pazoki, G. Boschloo, L. Kloo, Cation-Dependent Photostability of Co(II/III)-Mediated Dye-Sensitized Solar Cells. *The Journal of Physical Chemistry C* 119(44) (2015) 24704-24713, 10.1021/acs.jpcc.5b06310
- [19] Y. Li, J. Wang, H. Wang, Z. Di, M. Liu, X. Zong, C. Li, Y. Sun, M. Liang, Z. Sun, Transparent PEDOT counter electrodes for bifacial dye sensitized solar cells with cobalt complex mediator. *Chemical Communications* 59(90) (2023) 13482-13485, 10.1039/d3cc04037b
- [20] C. Hora, F. Santos, M. G. F. Sales, D. Ivanou, A. M. Mendes, Conventional and Back-Illuminated Cobalt- and Iodine-Mediated Dye-Sensitized Solar Cells for Artificial and Solar Light Conversion. *ACS Applied Energy Materials* 5(12) (2022) 14846-14857, 10.1021/acsaem.2c02307
- [21] Masud, M. Aftabuzzaman, H. Zhou, S. Kim, J. Yi, S. S. Park, Y. S. Kim, H. K. Kim, Chemically synthesized poly(3,4-ethylenedioxythiophene) conducting polymer as a robust electrocatalyst for highly efficient dye-sensitized solar cells. *Nanoscale* 16(29) (2024) 13874-13884, 10.1039/d4nr00949e
- [22] J. Capitão, J. Martins, S. Emami, D. Ivanou, A. Mendes, Fully glass frit encapsulated dye-sensitized solar cells: Challenges for hermetical sealing of electrolyte injection holes. *Solar Energy* 249 (2023) 476-484, 10.1016/j.solener.2022.12.001
- [23] J. Martins, S. Emami, D. Ivanou, A. Mendes, Ultralow Temperature Glass Frit Encapsulation for Stable Dye-Sensitized Solar Cells. *ACS Applied Energy Materials* 5(11) (2022) 14185-14192, 10.1021/acsaem.2c02714
- [24] F. Santos, J. Martins, J. Capitao, S. Emami, D. Ivanou, A. Mendes, Stable Cobalt-Mediated Monolithic Dye-Sensitized Solar Cells by Full Glass Encapsulation. *ACS Applied Energy Materials* 5(6) (2022) 7220-7229, 10.1021/acsaem.2c00765
- [25] F. Santos, D. Ivanou, A. Mendes, Solid-State Monolithic Dye-Sensitized Solar Cell Exceeding 10% Efficiency Using a Copper-Complex Hole Transport Material and a Carbon Counter-Electrode. *Solar RRL* 8(2) (2023) 2300574, 10.1002/solr.202300574
- [26] H. Ellis, N. Vlachopoulos, L. Häggman, C. Perruchot, M. Jouini, G. Boschloo, A. Hagfeldt, PEDOT counter electrodes for dye-sensitized solar cells prepared by aqueous micellar electrodeposition. *Electrochimica Acta* 107 (2013) 45-51, 10.1016/j.electacta.2013.06.005
- [27] A. Listorti, C. Creager, P. Sommeling, J. Kroon, E. Palomares, A. Fornelli, B. Breen, P. R. F. Barnes, J. R. Durrant, C. Law, B. O'Regan, The mechanism behind the beneficial effect of light soaking on injection efficiency and photocurrent in dye sensitized solar cells. *Energy & Environmental Science* 4(9) (2011) 3494-3501, 10.1039/c1ee01443a
- [28] J. Maçaira, L. Andrade, A. Mendes, Laser sealed dye-sensitized solar cells: Efficiency and long term stability. *Solar Energy Materials and Solar Cells* 157 (2016) 134-138, 10.1016/j.solmat.2016.05.016
- [29] A. Sacco, Electrochemical impedance spectroscopy: Fundamentals and application in dye-sensitized solar cells. *Renewable and Sustainable Energy Reviews* 79 (2017) 814-829, 10.1016/j.rser.2017.05.159
- [30] J. Gao, W. Yang, A. M. El-Zohry, G. K. Prajapati, Y. Fang, J. Dai, Y. Hao, V. Leandri, P. H. Svensson, I. Furó, G. Boschloo, T. Lund, L. Kloo, Light-induced electrolyte improvement in

- cobalt tris(bipyridine)-mediated dye-sensitized solar cells. *Journal of Materials Chemistry A* 7(33) (2019) 19495-19505, 10.1039/C9TA07198A
- [31] M. Bhagavathi Achari, V. Elumalai, N. Vlachopoulos, M. Safdari, J. Gao, J. M. Gardner, L. Kloo, A quasi-liquid polymer-based cobalt redox mediator electrolyte for dye-sensitized solar cells. *Phys Chem Chem Phys* 15(40) (2013) 17419-17425, 10.1039/c3cp52869c
- [32] A. Priyadarshi, L. J. Haur, P. Murray, D. Fu, S. Kulkarni, G. Xing, T. C. Sum, N. Mathews, S. G. Mhaisalkar, A large area (70 cm²) monolithic perovskite solar module with a high efficiency and stability. *Energy & Environmental Science* 9(12) (2016) 3687-3692, 10.1039/c6ee02693a
- [33] S. Castellano, H. Günther, S. Ebersole, Nuclear Magnetic Resonance Spectra of 2,2'-Bipyridyl. *The Journal of Physical Chemistry* 69(12) (1965) 4166-4176, 10.1021/j100782a018
- [34] N. Essayem, C. Lorentz, A. Tuel, Y. B. Tâarit, ¹H NMR evidence for the bi-pyridinium nature of the pyridine salt of H₃PW₁₂O₄₀. *Catalysis Communications* 6(8) (2005) 539-541, 10.1016/j.catcom.2005.05.006
- [35] F. Santos, C. Hora, D. Ivanou, A. Mendes, Efficient Liquid-Junction Monolithic Cobalt-Mediated Dye-Sensitized Solar Cells for Solar and Artificial Light Conversion. *ACS Applied Energy Materials* 4(5) (2021) 5050-5058, 10.1021/acsaem.1c00616